References

[1] Chapter, J. J., "Simplified Thermal Networks for the Lunar Module," *Journal of Spacecraft and Rockets*, Vol. 5, No. 10, Oct. 1968, pp. 1243–1245.

[2] Tawil, M. N. and Ferrara, A., "LM Flight Simulation in the Space Environment," AIAA Paper 69-991, Los Angeles, Calif., 1969.

[3] Chapter, J. J., "A Mathematical Description of the LM Glycol Loop Analog," LM Engineering Memo, LMO-510-568, April 1967, Grumman Aerospace Corp., Bethpage, N. Y.

[4] Chahine, N. T., "Performance Simulation Technique for the Lunar Module Environmental Control System," AIAA Paper 69-616, San Francisco, Calif., 1969.

[5] Connor, R. J. et al., "Adaption of Chrysler Improved Numerical Differencing Analyzer to CDC 6000 Series Computers," Engineering Department Technical Manual, M-68-22, Rev. 1, Nov. 1968, Martin-Marietta Corp., Denver, Colo.

[6] Grafton, J. C., "Transient Heat Transfer Analysis of Systems Involving Fluid Flow," ASD-TDR-620, North American Aviation, Downey, Calif. pp. 651–669.

Water Impact Accelerations of Axially Symmetric Bodies

YOICHI HIRANO* AND KORYO MIURA†
University of Tokyo, Meguro, Tokyo, Japan

Nomenclature

F = Froude number, Eqs. (4)
m = mass of body
m_v = virtual mass of water
v_0 = initial vertical velocity (impact velocity)
v = vertical velocity
h = displacement of body from free-water surface
t = time after instant of contact
ρ = mass density of water
r = radius of body in plane of water surface
R = radius of spherical bottom or characteristic length
θ = semivertex angle of cone
W = weight of body
δ, τ = nondimensional length and time, Eqs. (4)
μ = mass ratio, Eqs. (4)

Introduction

THIS study is concerned with the water impact of axially symmetric bodies. Water impact problems are important in some fields, especially in water-landing of seaplanes and of spacecraft. In 1929 von Kármán[1] derived the maximum impact loads of seaplane floats by applying the momentum theorem, and since then many investigations have been made for wedges entering the water surface. Studies of the water landing problems of spacecraft have been made recently at NASA Langley Research Center.[2,3] The object of these studies seems to have been to determine the practical design loads during the water impact of the particular spacecraft, and this objective was accomplished. However, they did not present the general formulas for the impact accelerations supported by systematic experiments.

This Note presents analytical and experimental results on impact accelerations of axially symmetric bodies landing on water. The formulas for the maximum impact accelerations are derived using the momentum theorem. The experimental results of spherical and conical models are presented and compared with the analytical results.

Received January 21, 1970; revision received February 27, 1970.

* Assistant, Institute of Space and Aeronautical Science.

† Associate Professor, Institute of Space and Aeronautical Science. Member AIAA.

Table 1 Spherical and conical models

Sphere	Radius, mm	Wt, kg A[a]	Wt, kg B[b]
S-1	239	1.429	1.399
S-2	203	1.374	1.344
S-3	156	1.300	1.270

Cone	Semivertex angle, deg	Wt, kg
C-1	65	1.530
C-2	60	1.383
C-3	55	1.349

[a] With a 100 g accelerometer.
[b] With a 200 g accelerometer.

Analysis

The original momentum of the body is assumed to be distributed between the body and the water during the impact.[1] From the momentum theorem the following equation can be written.

$$mv_0 = (m + m_v)v \tag{1}$$

The body considered has the axially symmetric bottom surface. We propose that the virtual mass for axially symmetric body be taken equal to one-half the virtual mass of a circular plate having a diameter equal to the instantaneous diameter of the body in the plane of the water surface. The virtual mass of the circular plate is given by Lamb[4] as

$$m_v = \tfrac{8}{3}\rho r^3 = (2/\pi)(\tfrac{4}{3}\pi\rho r^3) \tag{2}$$

For the spherical bottom surface, the virtual mass can be written as

$$m_v = \tfrac{4}{3}\rho h^{3/2}(2R - h)^{3/2} \tag{3}$$

The following nondimensional parameters are now introduced:

$$\delta = h/R,\ \tau = gt/v_0,\ F = v_0/(gR)^{1/2},\ \mu = 3W/4\pi\rho gR^3 \tag{4}$$

Substituting Eq. (3) into Eq. (1) gives

$$d\delta/d\tau = \mu F^2/[\mu + \delta^{3/2}(2 - \delta)^{3/2}/\pi] \tag{5}$$

If $\delta \ll 1$, Eq. (5) is easily integrated to yield

$$\tau = (\delta/\mu F^2)\ [\mu + (2^{5/2}/5)(1/\pi)\delta^{3/2}] \tag{6}$$

The acceleration can be calculated as

$$d^2\delta/d\tau^2 = -[3 \times 2^{1/2}\mu^2 F^4 \delta^{1/2}/\pi(\mu + 2^{3/2}\pi^{-1}\delta^{3/2})^3] = -F^2 n \tag{7}$$

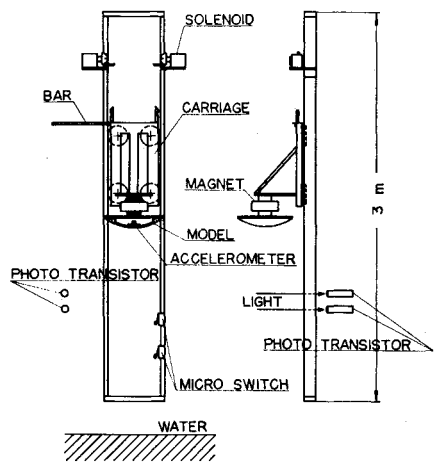

Fig. 1 Test apparatus.

Table 2 Experimental and theoretical results: spherical (S) and conical (C) models

Model	v_0, m/sec	Experimental n'_m, g	Experimental n_m, g	Experimental t_m, msec	Theoretical n_m, g	Theoretical t_m, msec
S-1	3.06	67.1	27.0	2.99	23.0	1.88
	3.94	144	42.8	2.69	38.7	1.44
	4.74	210	57.8	2.68	55.9	1.20
S-2	3.06	80.1	24.2	2.40	20.0	2.16
	3.93	103	36.4	2.32	33.1	1.68
	4.74	177	51.8	1.43	48.8	1.37
S-3	3.01	38.4	18.1	2.99	15.5	2.68
	3.95	58.6	27.7	2.23	26.7	2.04
	4.74	81.8	37.4	2.20	38.3	1.70
C-1	2.97	...	11.9	9.72	11.3	11.6
	3.78	...	18.3	7.67	18.3	9.10
	4.75	...	28.9	6.60	28.9	7.23
	5.33	...	38.4	5.90	36.3	6.45
C-2	2.91	...	9.09	11.9	9.07	14.2
	3.80	...	15.1	8.33	15.4	10.8
	4.61	...	22.8	7.13	22.7	8.95
C-3	2.91	...	7.16	12.1	7.51	17.1
	3.90	...	12.0	10.0	13.5	12.8
	4.77	...	18.1	8.77	20.2	10.5

The maximum acceleration is

$$(d^2\delta/d\tau^2)_m = -\tfrac{256}{248}\pi^{-2/3}\mu^{-2/3}F^4 = -F^2 n_m \quad (8)$$

when

$$\delta_m = \pi^{2/3}\mu^{2/3}/8 \quad (9)$$

Substituting Eq. (9) into Eq. (6) yields

$$\tau_m = (21\pi^{2/3}/160)(\mu^{2/3}/F^2) \quad (10)$$

For the conical bottom, the virtual mass can be written as

$$m_v = 4\rho h^3 \tan^3\theta/3 \quad (11)$$

where θ is the semivertex angle of the cone.

Using the same procedure as before, the equations for the conical case are obtained:

$$n = 3\tan^3\theta\mu^2F^2\delta^2/\pi[\mu + (\tan^3\theta\delta^3/\pi)]^3 \quad (12)$$

$$\tau = (1/\mu F^2)\ [\mu\delta + (\tan^3\theta/4\pi)\delta^4] \quad (13)$$

$$n_m = [(7^{7/3} \times 2^{2/3})/3^5\pi^{1/3}]\tan\theta\mu^{-1/3}F^2 \quad (14)$$

$$\tau_m = (2\pi/7)^{1/3}(\tfrac{15}{14})(\mu^{1/3}/F^2\tan\theta),\ \delta_m = (2\pi/7)^{1/3}\mu^{1/3}/\tan\theta \quad (15)$$

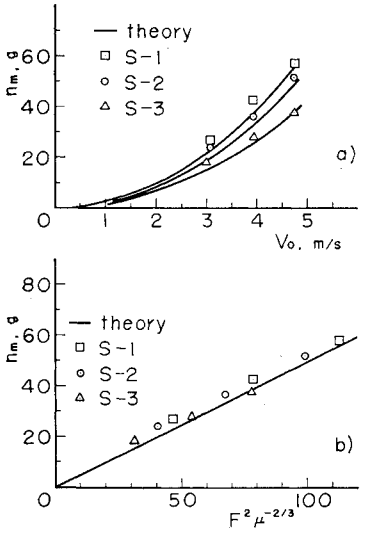

Fig. 2 Spherical bottom: a) maximum faired acceleration vs contact velocity, b) comparison of data with Eq. (15).

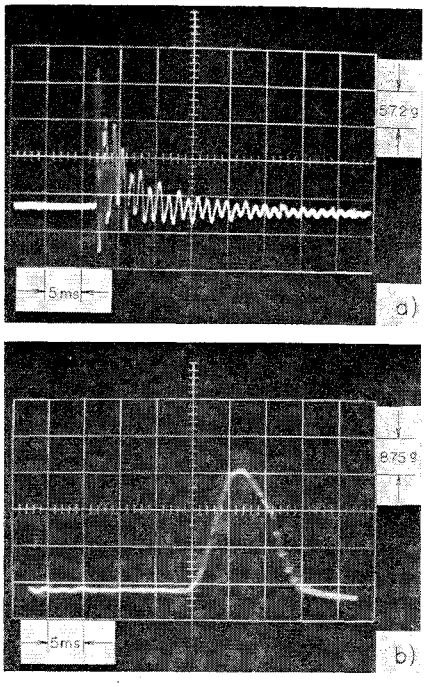

Fig. 3 Acceleration-time histories: a) spherical bottom (S-1, $v_0 = 4.74m/s$), b) conical bottom (C-1, $v_0 = 4.74m/s$).

For the general axially symmetric bodies the same analytical procedure can be applied.

Experimental Procedures

Six models used were made of acetal copolymer and had the spherical or conical bottom surfaces, the dimensions of which are presented in Table 1.

The test apparatus is shown in Fig. 1. A model was attached to the electrical magnet of the carriage. The carriage was released from the predetermined height, and the model was dropped into a free-fall at the lowest point of the guide rail by cutting the electrical current of the magnet. The velocity of the carriage at the lowest point was measured by recording the time for travelling the last 7.7 cm of the guide rail. The time was recorded by an electronic counter, and the water contact velocity of the model was calculated by considering the free-fall height (15–19 cm), which was

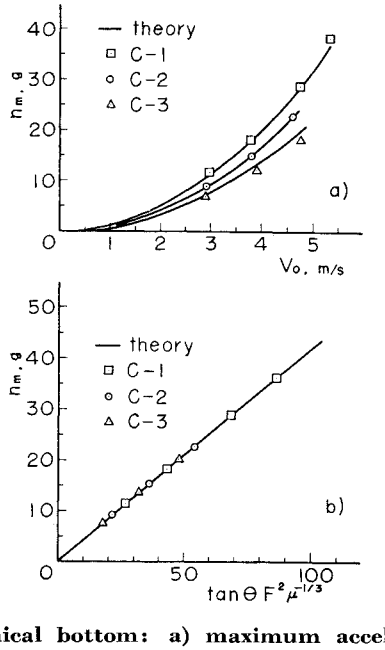

Fig. 4 Conical bottom: a) maximum acceleration vs contact velocity, b) comparison of data with Eq. (21).

the height between the model-release point and the water surface.

The accelerations were measured by strain-gage type accelerometers, and the records were traced on an oscilloscope and photographed. The two accelerometers used were a ± 100 g Kyowa accelerometer with a natural frequency of 2000 cps and a ± 200 g accelerometer with a natural frequency of 3000 cps. Both were damped to 65% of critical damping. A Kyowa amplifier was used which had a carrier frequency of 20,000 cps.

Experimental Results

The tests were repeated 3–5 times each, and the measured values of v_0, n_m, and τ_m scatter within 5% of the mean value. Therefore the mean values are used for the comparison with the analytical results.

The experimental results and the comparison with the theoretical values for the spherical models are presented in Table 2 and Fig. 2. An acceleration-time history curve is shown in Fig. 3a. This photographic record shows the oscillatory characteristics of the acceleration which may be attributed to the bottom structural elasticity. Therefore two types of the maximum acceleration were derived, a maximum faired acceleration[3] (n_m) and a pure maximum acceleration (n'_m). The faired acceleration is supposed to correspond to the acceleration of the rigid body by the experiments, which compared the two models of the identical configuration and weight but with the different structural elasticity.

The results for the conical models are presented in Table 2 and Fig. 4. The theoretical values were calculated using Eqs. (14) and (15). An oscilloscope trace is shown in Fig. 3b. The agreements between the experimental and the theoretical values are very good.

Conclusion

The formulas for the maximum water impact accelerations of the spherical and conical bodies have been derived in the closed form. The experiments were carried out systematically to check the analytical results. The agreements between the experimental and the theoretical values are quite satisfactory. A further theoretical study is desirable to clarify the oscillatory phenomena of the acceleration-time history observed in the experiments.

References

[1] von Kármán, T., "The Impact on Seaplane Floats during Landing," TN 321, 1929, NACA.

[2] McGehee, J. R., Hathaway, M. E., and Vaughan, V. L., "Water-Landing Characteristics of a Reentry Capsule," MEMO 5-23-59L, June 1959, NASA.

[3] Stubbs, S. M. and Hathaway, M. E., "Effects of Bottom-Structure Flexibility on Water Landing Loads of Apollo Spacecraft Models," TN D-5108, March 1969, NASA.

[4] Lamb, H., *Hydrodynamics*, 6th ed., Cambridge Univ. Press, Cambridge, Mass., 1932.

Prediction of Terminal Variables in Homing

A. G. Rawling*
General Electric Company, King of Prussia, Pa.

Nomenclature

A = azimuth angle of velocity vector
LOS = line-of-sight connecting missile and target
M = miss distance at some specified time
R = range between missile and target along the line of sight
t = real time
V = flight velocity or speed
x,y = Cartesian coordinates
θ = angle that the relative velocity vector makes with the line of sight
σ = line of sight angle measured with respect to a fixed inertial direction in the plane

Superscripts

$(\dot{})$ = $d(\ )/dt$
$(\bar{})$ = bar denotes vector

Subscripts

0 = initial conditions existing at time $t_0 = 0$
e = conditions existing at time t_e of $\ddot{\sigma}$ first extreme
g = conditions existing at "time-to-go" t_g
I = inertial
i = conditions existing at time t_i of $\ddot{\sigma}$ first inflection point
M = missile
T = target
R = relative (as in relative velocity $\bar{V}_R$)
w = conditions existing at "time-to-pass" t_w

Introduction

THE predicted terminal behavior of passive kinematic variables such as the line of sight angle, its rate, and its acceleration (as well as the active variables range and range rate) is of major importance in rendezvous, inspection, and interception. Direct application can be made to the fields of fuzing on target and/or countermeasures, directional warhead aiming (in addition to safing, arming, and self-destruction), timely deployment of submissiles, adaptive control of onboard data processing parameters, physical homing simulators, and proper design of tracking systems and seeker gimbal mountings.

Terminal behavior is assumed herein to describe the tactical situation existing during the final closing moments of interception when the missile is unable to execute promptly any significant guidance command, as a result of hardware limitations, time lags, or inertial mass. In such a case, mission considerations may still dictate that the tracking system be able to retain the target within the sensor field of view. In addition, error comparison between measured variables and their onboard predicted values may be used to actuate devices and control ordered sequences of interrelated actions.

It is the twofold purpose of this Note to supply both qualitative and quantitative information on the terminal behavior of the kinematic variables during the interception final phase. Explicit expressions are given for the quantities as functions of time and their corresponding graphical over all behavior is shown. In addition, their predicted terminal values at the future instant of closest separation are given as functions of existing measurements taken at the time of observation.

Although all expressions given are for the case of two-dimensional planar interception, this situation is closely approximated in three dimensions by the inclined plane of interception defined by the missile and target velocity vectors in the terminal homing phase.

Kinematics

Figure 1 combines two distinct but related coordinate systems for depicting interception by a point missile and target both flying constant speed, rectilinear flight paths in the plane. Absolute Cartesian coordinates, denoted by the fixed inertial axes (x_I,y_I), are imposed on the physical situation, with both target and missile moving for $t > t_o = 0$, and the resulting action is shown above the initial LOS in Fig. 1.

For relative coordinates, with the ensuing action shown below the LOS, the target is considered fixed at its initial position, with the missile flying a path defined in direction by the relative velocity vector (and with that same speed).

Received February 27, 1970.

* Consulting Engineer, Guidance, Re-Entry and Environmental Systems Division. Member AIAA.